water

MDPI

Article

Forensic Investigation of Four Monitored Green Infrastructure Inlets

Leena J. Shevade [1] and Franco A. Montalto [2,*]

[1] Civil and Environmental Engineering Department, Lafayette College, Easton, PA 18042, USA; shevadel@lafayette.edu
[2] Civil, Architectural & Environmental Engineering Department, College of Engineering, Drexel University, Philadelphia, PA 19104, USA
* Correspondence: fam26@drexel.edu

Abstract: Green infrastructure (GI) is viewed as a sustainable approach to stormwater management that is being rapidly implemented, outpacing the ability of researchers to compare the effectiveness of alternate design configurations. This paper investigated inflow data collected at four GI inlets. The performance of these four GI inlets, all of which were engineered with the same inlet lengths and shapes, was evaluated through field monitoring. A forensic interpretation of the observed inlet performance was conducted using conclusions regarding the role of inlet clogging and inflow rate as described in the previously published work. The mean inlet efficiency (meanPE), which represents the percentage of tributary area runoff that enters the inlet was 65% for the Nashville inlet, while at Happyland the NW inlet averaged 30%, the SW inlet 25%, and the SE inlet 10%, considering all recorded events during the monitoring periods. The analysis suggests that inlet clogging was the main reason for lower inlet efficiency at the SW and NW inlets, while for the SE inlet, performance was compromised by a reverse cross slope of the street. Spatial variability of rainfall, measurement uncertainty, uncertain tributary catchment area, and inlet depression characteristics are also correlated with inlet PE. The research suggests that placement of monitoring sensors should consider low flow conditions and a strategy to measure them. Additional research on the role of various maintenance protocols in inlet hydraulics is recommended.

Keywords: stormwater green infrastructure performance; forensic investigation of GI; monitoring green infrastructure performance; sustainable urban water management

Citation: Shevade, L.J.; Montalto, F.A. Forensic Investigation of Four Monitored Green Infrastructure Inlets. *Water* **2021**, *13*, 1787. https://doi.org/10.3390/w13131787

Academic Editors: Ryan Winston and Peter Weiss

Received: 16 April 2021
Accepted: 17 June 2021
Published: 28 June 2021

1. Introduction

As cities grow, existing infrastructure will become increasingly stressed, with potential negative impacts on the environment, including habitat losses. Rapid urbanization and extreme weather due to climate change can increase water-related challenges such as flooding, groundwater exploitation, scarcity, and pollution [1]. For this reason, restoration and improvement of urban infrastructure is already one of the 14 nationally and internationally recognized grand challenges for engineering (NAE, 2008) [2]. Urban infrastructure needs to be smart, sustainable, and resilient to various stressors found in today's cities. Urban water management is a crucial component in the planning of sustainable cities, especially in the context of population growth and urbanization.

The urban drainage system is an essential component of a city's infrastructure, with direct implications for flood control, stormwater management, and public health. Green infrastructure (GI) is a distributed approach to urban drainage that seeks to retain and detain stormwater in a decentralized manner. Its rapid rate of implementation is currently outpacing the rate at which research comparing the performance of alternative designs has been performed [3], and there is a great need for research documenting how different kinds of GI perform under a range of precipitation [4,5] and site conditions.

Performance can be evaluated through in situ monitoring of built GI subject to various climatological and geomorphological characteristics such as hydraulic loading ratios, street slopes, underlying geology, and soil mix. Though monitoring is the most comprehensive method to evaluate the performance of individual GI systems, it is expensive, tedious, and time-consuming and the results can be highly uncertain due to a lack of experimental control [6]. Thus, relative to the thousands of GI sites already built in New York City (NYC), only a small number will ever be equipped with the equipment needed to characterize hydraulic and hydrologic (H&H) performance. To augment the benefits achieved through field monitoring at individual sites, side-by-side studies can be performed to isolate the difference in GI performance due to specific design parameters. The results of these comparative field studies can then be used with physical or statistical models to quantify the effect of these design parameters under a range of other conditions. Thus, computer models can be used to contextualize and to generalize the results of individual performance monitoring efforts, and to also quantify the uncertainty associated with variable site and climatic conditions.

Previous GI research has focused on the roles that design parameters such as media depth, underdrain, in situ soil, and soil characteristics [7–9] on hydrological performance. The extent to which hydrological processes such as infiltration [10–12] and evapotranspiration [13] alter the hydrological performance of GI systems has also been studied. The hydraulic loading ratio (HLR), defined as the ratio of tributary catchment area associated with the GI to the area of GI, was also found to be positively correlated to GI performance by increasing evapotranspiration [14]. GI inlet design and its performance are understudied.

One of the studies focusing on this phenomenon in GI systems [15] reported highly variable performance from event to event and underutilization of the depression storage of a streetscape bioretention system in Queens, NY over 92 monitored storms occurring over four years. The site captured an average of 72% of all runoff generated within its tributary area during the monitored events, with the remainder assumed to have bypassed the inlet.

This paper provides a forensic interpretation of the potential role of apron slopes, inlet clogging, and inflow rate in determining monitored inlet efficiency, applying insights and conclusions presented in the previous study, Shevadel et al. (2020) [16]. The analysis focuses on four inlets at two different GI sites in NYC.

This research could help to (i) inform design protocols; (ii) prescribe a static engineered storage capacity required to capture a particular target event depth in a GI facility installed within a specific hydrologic, morphologic, and geologic context; and (iii) predict the stormwater capture performance of constructed facilities. This kind of research can also be used to upscale site-specific findings to the watershed scale.

2. Materials and Methods

2.1. Site Characteristics

Monitoring data were collected at two sites: the Nashville green street (40.84–73.88), which had one monitored inlet, and the Happyland green street (40.69–73.76), which had three inlets as shown in Figure 1. Figure 1a presents a photograph of the inlet and flume at the Happyland SW inlet at Happyland site. The details of the inlets and the monitoring setup for flow measurement at Happyland, which has three inlets (referred to as SW, SE, and NW), are portrayed in Figure 1b. Figure 1c presents a photograph of the inlet and flume at the Nashville (referred to as Nash) site. The details of the Nashville site are portrayed in Figure 1d. Each inlet was equipped with an extra-large 60° V–Trapezoidal Flume. The inlets were designed to have free-outfall conditions into the green street. The bottom of the flume into the green street was 15 cm above the soil layer and the grating near the inlet diverted the inflow rapidly away from the inlet, maintaining free outfall conditions.

(**a**)

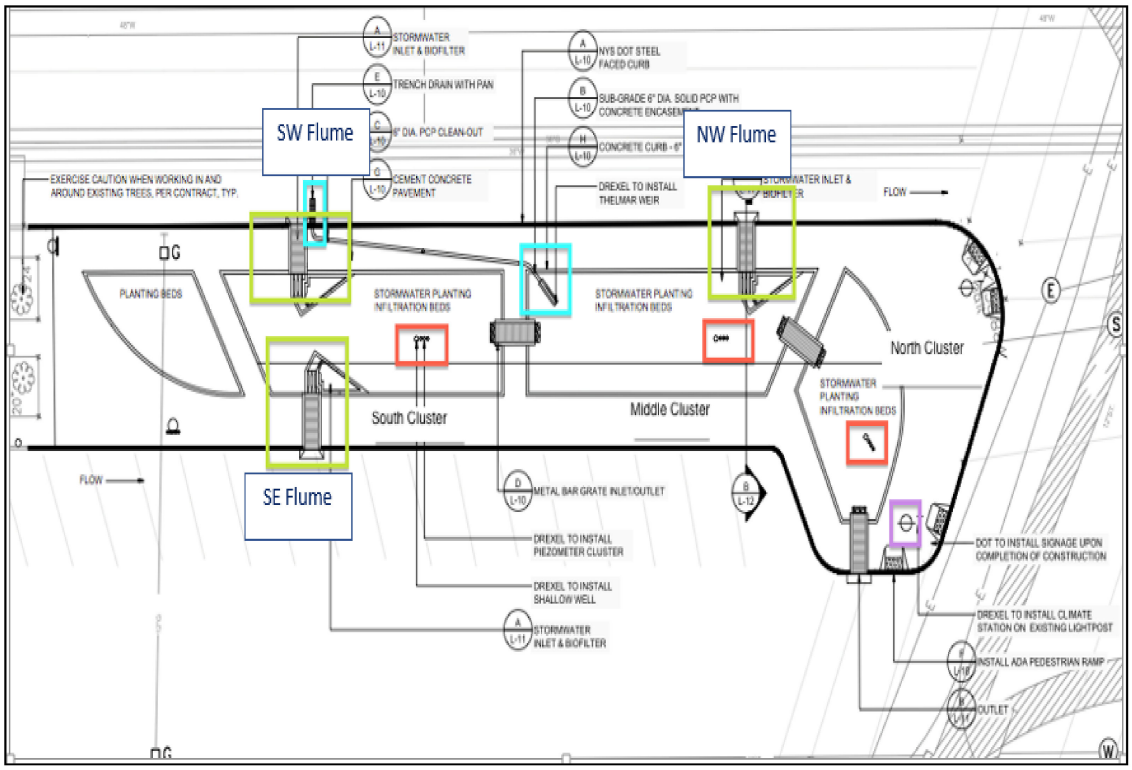

(**b**)

Figure 1. *Cont.*

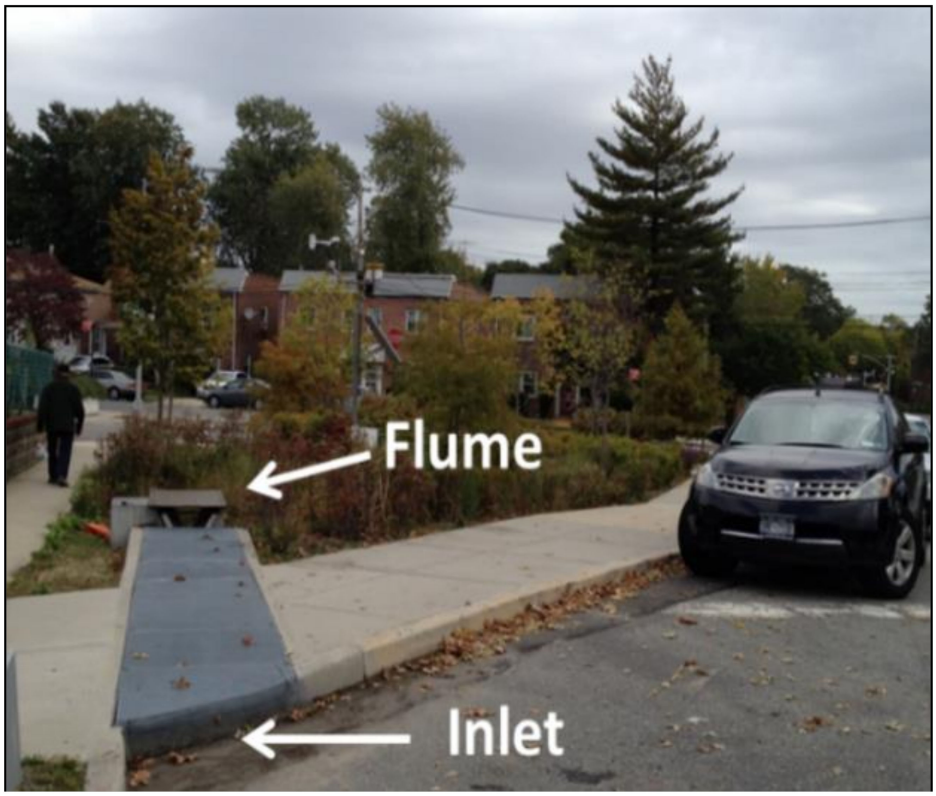

(**c**)

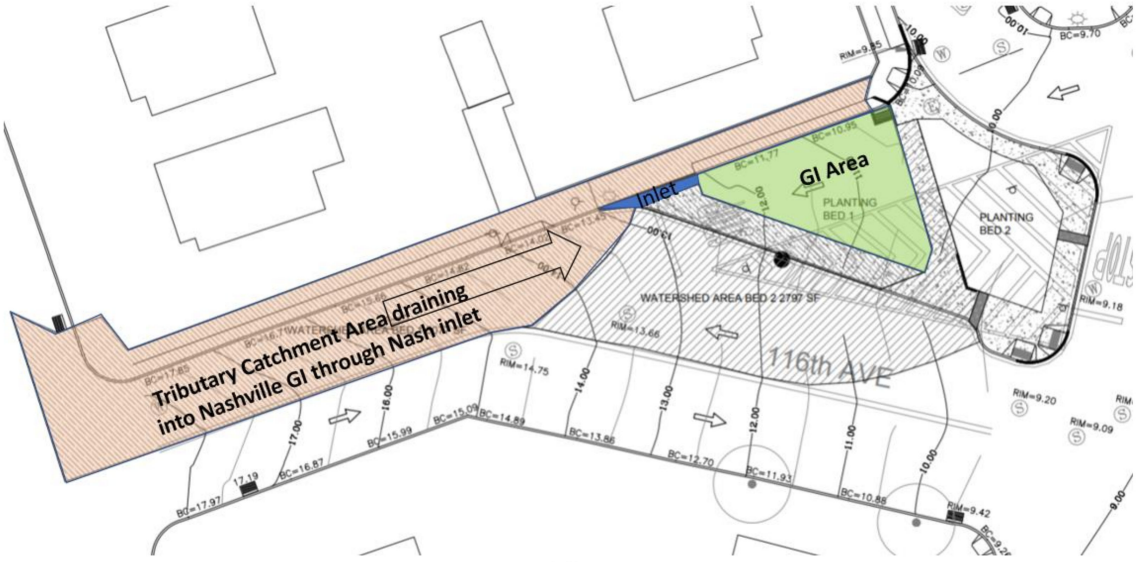

(**d**)

Figure 1. Inlets considered in this investigation. (**a**) photograph of SW inlet (shown by white arrow) at Happyland green street; (**b**) locations of three inlets on design drawing (plan view) of Happyland green street; (**c**) photograph of inlet at Nashville green street; and (**d**) the locations of the inlet and tributary catchment area on design drawing (plan view) of Nashville green street.

The other site characteristics such as tributary catchment area, street slopes (slope of tributary catchment area), and hydraulic loading ratio for each inlet are also included in Table 1. All four inlets were rectangular curbcuts of 0.82 m inlet length that discharged into a rectangular channel connected to a flume. The outlet of each flume discharged into a shallow settling basin designed to trap sediment.

Table 1. Site characteristics.

Site	Happyland NW	Happyland SE	Happyland SW	Nashville (Nash)
Tributary catchment area (m^2)	325.16	278.7	650.3	475
GI area (m^2)	99.03	99.03	102.94	125
Longitudinal slope (%)	1.29	1.12	1.19	3.75
Transverse slope (%)	1.15	0.75	1.51	4.37
Hydraulic loading ratio (HLR)	3.28	2.81	6.32	3
Depth of ponding (m)	0.15	0.15	0.15	0.15
Inlet type	Curbcut with depression	Curbcut with depression	Curbcut with depression	Curbcut on grade

The tributary catchment area is the area of street draining into the inlet and is depicted in Figure 1d.

2.2. Monitoring Setup

The sites were monitored between 2015 and 2017 using onsite tipping bucket rain gauges, pressure transducers, and flumes, with data logged at five-minute time intervals. The monitoring setups at each site are described in Table 2.

Table 2. Monitoring setup at site.

Equipment	Specifications
Data logger	CR 1000
Rainfall	TE525MM-L (0.1 mm rainfall per tip, 1.0% up to 50 mm/h, and 24.5 cm orifice diameter)2 gauges at site and 2 control gauges (for verification)
Inflow	3 Tracom Flumes (60° Trapezoidal—Extra-Large V-Notch) Campbell Scientific CS451 Pressure Transducer (0–5 m range with ±0.005 m)

2.2.1. Precipitation

Precipitation data were collected using a pair of TEM525MM-L 0.254 mm tipping bucket rain gauges (Texas Electronics) with a standard accuracy of 1% at rainfall intensities of up to 50 mm/h. Dual rain gauges provided some redundancy to reduce the potential for systematic error, to help to ensure a continuous data stream given the anomalous behavior (absence of records, signs of blockage, etc.) intrinsic to tipping buckets [17,18], and to reduce the potential for random errors that can be achieved by averaging two or more collocated rainfall measurements [18]. The gauges were installed on poles, and not in pits, to lower the probability of their being damaged by pedestrian or vehicular traffic or surface floods. The rain gauges were installed at 3.65 m above the ground, following recommendations of the World Meteorological Organization (2010) [19]. The rain gauges were not heated; hence, winter data were excluded from analysis. The sampling interval for all sensors was 10 s, with rain amounts from consecutive sampling periods summed into 5 min logged totals that were transmitted in real time to a server using cellular modems. Maintenance of the rain gauges was performed biweekly; any debris was removed immediately.

Rain gauges were factory calibrated, and in situ calibration was performed annually using the "soda bottle test", which involves counting the number of bucket tips that occur as a known volume of water is dripped into the tipping bucket through a small hole in a soda bottle. This number of tips is then compared to the reference tips for that volume provided by the manufacturer to verify the accuracy of the measurements.

2.2.2. Depth of Flow

Tracom Extra-Large 60-Degree V-Notch Trapezoidal Flume was attached at the end of the channel. All flumes were fitted with Campbell Scientific CS451 Pressure Transducers that

were factory calibrated, and loggers were programmed to read water depth. A photograph of a flume, a pressure transducer holder, and a street curbcut is presented in Figure 2.

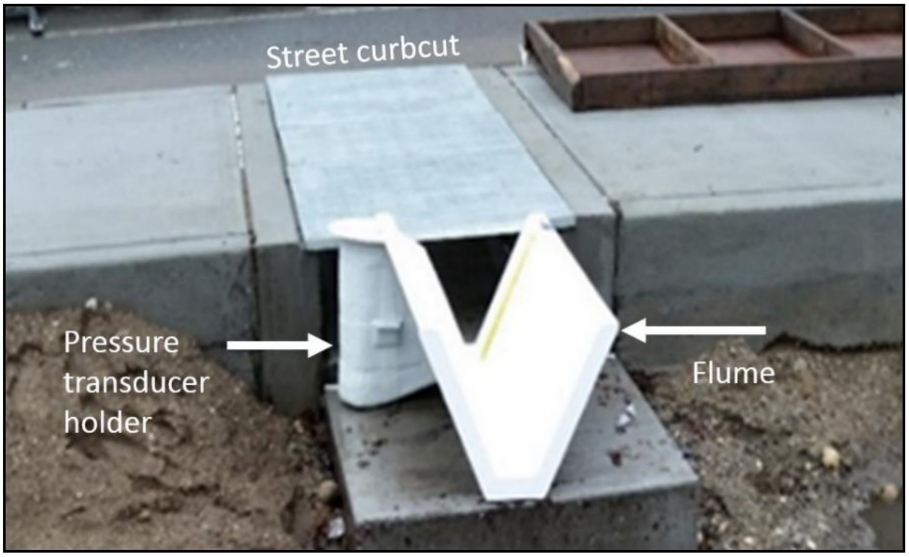

Figure 2. Curbcut inlet fitted with flume and pressure transducer for flow measurement.

The pressure transducers were initially factory calibrated, but their logged data were periodically verified against manually surveyed data in the field. The relationship between observed and sensor recorded flow depths was represented by a linear equation y = mx + b, where y is the actual water depth and x is the corresponding depth recorded by the pressure transducer. The standard error of these equations in reproducing the full set of calibration data was then computed (Table 3).

Table 3. Calibration curves for all pressure transducers used to measure water level.

Year	Pressure Transducer	Equation	Standard Error	Number of Data Points (N)
2015 (New Sensors)	NW	y = 1.0092x + 0.0117	0.0019	07
	SE	y = 1.0251x + 0.0124	0.0093	07
	SW	y = 0.9942x + 0.0158	0.0260	07
	Nashville	y = 0.7318x + 0.0044	0.0012	07
2016	NW	y = 1.0151x + 0.0055	0.0019	14
	SE	y = 1.0782x + 0.0105	0.0091	14
	SW	y = 1.183x + 0.0494	0.0269	14
	Nashville	y = 0.9984x + 0.0049	0.0273	14
2017	NW	y = 0.6197x + 0.1976	0.0115	14
	SE	y = 1.1189x + 0.0096	0.0068	14
	SW	y = 1.0035x + 0.0055	0.0051	14
	Nashville	y = 1.0381x + 0.0234	0.0145	14

2.3. Data Analysis

2.3.1. Precipitation—Event Separation

The 5 min homogenized precipitation data were disaggregated into individual events using a 4 h inter-event dry period. A minimum of 4 mm of total depth of precipitation was necessary to define an event, as a depth corresponding to the minimum runoff flowrates that could be measured at the inlets using a pressure transducer. The precipitation events that occurred at both sites are considered in the analysis. Event IDs are generated based on the start date of an event. The Event ID refers to the precipitation on the same day at both sites.

2.3.2. Estimation of Presented Flowrate to the Inlet

The rate of runoff generated in the tributary areas and presented to the inlets was not measured directly. Instead, onsite precipitation data were used with an EPA Stormwater Management Model (SWMM) Version 5.1.013 [20] of the tributary drainage area to develop a runoff hydrograph for each event at each inlet. Physical conditions needed to represent the tributary area characteristics (e.g., size and geometry of the tributary area, slopes, surface condition, etc.) were surveyed in the field.

The time series of flow into the model outlet is the approximation of tributary runoff used in the analysis. In the models, the street was represented as 100% impervious tributary catchment areas, with other properties as listed in Table 4.

Table 4. Parameters used in SWMM runoff modeling.

Site	Definition as Per SWMM 5.1 Manual [20] along with Description	Happyland	Happyland	Happyland	Nashville
		NW	SE	SW	(Nash)
Tributary catchment area (Hectare)	The area of street draining into the inlet is depicted in Figure 1d.	0.325	0.278	0.650	0.475
Catchment width (m)	Catchment width is the average of maximum flow lengths (feet or meters).	10.31	2.99	7.84	10.45
Maximum flow length (m)	Longest flow length	31.53	93.21	82.94	45.45
Catchment area slope (%)	Average % slope of the street section in longitudinal direction.	1.29	1.12	1.19	3.75
% Impervious	The entire catchment upstream of inlet is impervious.	100	100	100	100
N—Impervious	Manning's n for overland flow over the impervious portion of the sub-catchment (0.011–0.024 for asphalt, concrete, or cement rubble street surface for overland flow or for open channel).	0.02	0.02	0.02	0.02
D—Store impervious	The runoff from the street was directed directly to the outlet (physically, that is the inlet to the GI area).	0.05	0.05	0.05	0.05
% Routed	As per design, the entire tributary catchment area is draining into the inlet. Thus, 100% of the tributary catchment area is routed outlet (physical inlet).	100	100	100	100
Sub-area routing		To outlet	To outlet	To outlet	To outlet

2.3.3. Intercepted Flowrate Measurements

The flow depths measured in the flumes were converted into flowrates using stage–discharge curves provided by the flume manufacturer. These curves were verified by the research team, in situ, during simulated runoff tests performed with a fire hydrant. These tests identified the manufacturer-specified position to read the water level and the PT installed in the stilling well had offset. It was 2 mm for Nashville and 6.35 cm for Happyland. A mathematical representation of this curve is provided in Equation (1).

$$Q_{int}(CMS) = 0.8681 \times \left(H_{flume}^{2.5553}\right) \quad (1)$$

where H_{flume} (m) is the calibrated 5 min pressure transducers (PT) depth (minus the 6.35 cm offset between the PT elevation and the flume throat for Happyland and 2 mm for Nashville) measured in m, and Q_{int} is the discharge associated with that depth in cubic feet per second, per the stage–discharge relationship provided by the manufacturer.

2.4. Forensic Investigation

The results of the quantitative analysis with field measurements were verified with onsite observations. The contour plots developed in Shevade et al. (2020) [16] using a CFD model validated with field-collected data were used to perform forensic investigations on the monitoring data. The contour graphs Figures A1 and A2 developed in that study are presented in Appendix A for ready reference.

2.5. Summary of Data Quality Protocol

Each site was fitted with a pair of rain gauges for redundancy. Precipitation data were collected at 5 min intervals, and an R code was written to quality control the data. To distinguish between an error and no rain, a threshold of 1 mm of total precipitation was established as the minimum recordable rainfall amount to avoid measurement errors due to wind, bird droppings, or other random occurrences. To remedy the fact that the data logger occasionally misses time steps and/or logs at random intervals, part of the R code homogenizes the data to generate a continuous time series of five-minute time-stamped values. Observed data gaps were filled with zero values during dry periods. Data from individual gauges at each site were compared with data from other monitored sites to identify the working and non-working rain gauges, as well as continuously over predicting or under predicting rain gauges (systematic errors).

A summary of the quality assurance and quality check (QA/QC) protocols described above is included in Table 5. In addition to the protocols already described, visual inspections of the site and data were performed regularly. Outliers, noise, and other anomalous conditions were flagged and remedied.

Table 5. QA/QC criteria.

Quality Tag	Description	Action
Criterion #1	Inconsistent time step (same for both precipitation and inflow)	- Round to nearest five-minute data interval
Criterion #2	Precipitation data gap	- Fill dry weather gap with zero - During the event, verify precipitation data with other rain gauges at the same station
Criterion #3	Precipitation data gap	- Fill dry weather gap with zero - Verify precipitation data with rain gauge at other station and/or NOAA reference stations
Criterion #4	Inflow data gap	- Fill dry weather gap with last reading - Data gap > 10 min, discard the event - Data gap < 10 min, interpolate intermediate data
Criterion #5	Random spikes or dips in the precipitation and inflow data (can happen due to auto-reset of sensor or logger)	- Spike or dip longer than one data interval, discard the event - Interpolate intermediate data
Criterion #6	If post-calibration water level data in the flume are above the depth of the curb	- Consider water level as maximum possible depth in the flume

The following assumptions were made while calculating runoff flowrate and intercepted flowrates.

a. Upper bounds for flowrates:

Based on the stage–discharge curve provided by the manufacturer for the maximum inlet depth of 0.154 m, the inlet can discharge 0.007 CMS. Thus, the 0.007 CMS flowrate is the maximum possible value of intercepted flowrate. All computed intercepted flowrates

greater than this maximum discharge capacity (>0.007 CMS) for the inlet were considered physically impossible.

b. Additional catchment area draining during high-intensity storms:

The presented flowrates were calculated based on the design tributary catchment area. However, during the field investigations, the research team determined that precise definition of the tributary catchment area is not possible due to complex undulations in the street and sidewalk surfaces. Significant uncertainty is attributed to the drainage area estimate and data sets like runoff, which are derived from it.

c. Identification of model and/or measurement uncertainty:

The pressure transducer data are affected by the occasional deposition of debris in the flume and inlet channel. In addition to the calibration equation developed at the site, a curation protocol was adopted to process the water level raw data. Moreover, and because the two onsite rain gauges sometimes did not record similar values for the same events, two additional reference rain gauges, located 0.5 km from the sites, were included in the study. Precipitation was assumed to be the average of the values recorded at all four gauges, and this value was input into the SWMM model to compute the presented flowrate time series. This procedure was determined to generate presented flowrates that better matched the inflow when compared to those modeled using one of the onsite rain gauges.

d. Data curation:

Theoretically, the raw pressure transducer reading should read zero at the beginning and end of the event, while during the event, as the flume receives water, the pressure transducer reading should be non-zero. In practice, this was not always the case, and the readings were adjusted as such by subtracting the initial pre-rain reading from all the readings during the event, in a curation process. In addition to the pressure transducer calibration equation, this adjustment parameter was derived based on the minimum and maximum possible value of water level set to obtain curated time series.

2.6. Inlet Performance Metric

Inlet capacity is defined as the maximum presented flowrate that can be completely intercepted by the inlet [21]. When the presented flowrate exceeds the inlet capacity, inlet bypass is presumed to have occurred.

The efficiency of the inlet during both the observed and simulated conditions was evaluated using Equation (2): the inlet efficiency (E) [21] defined as the ratio of intercepted flow by the inlet Q_{int} to the approaching inflow Q at steady state:

$$E(\%) = \frac{Q_{\text{int}}}{Q} \times 100 \tag{2}$$

E can vary between 0% and 100%, with 0% indicating no flow into the inlet, and 100% representing interception of all presented flow.

To evaluate the inlet performance during a precipitation event, two metrics were developed. The mean inlet efficiency provided information on the average inlet performance during the event whereas the peak inlet efficiency provided information about inlet performance for the time period during the event when the inlet was presented with peak flowrates during a particular event.

The mean inlet efficiency (*Mean E*) for an individual event is calculated by Equation (3).

$$Mean\ inlet\ Efficiency(MeanE)(\%) = 100 \times \frac{Mean\ intercepted\ flowrate(Qmean\_int)}{Mean\ presented\ flowrate(Qmean\_presented)} \tag{3}$$

where *mean intercepted flowrate* is calculated by averaging all intercepted flowrates observed during that event and the *mean presented flowrate* is calculated by averaging all expected

flowrates derived from the SWMM model using tributary drainage area characteristics as per design drawings.

The peak inlet efficiency (*Peak E*) for an individual event is calculated by Equation (4).

$$Peak\ inlet\ eficiency(PeakE)(\%) = 100 \times \frac{Peak\ intercepted\ flowrate(Qpeak\_int)}{Peak\ presented\ flowrate(Qpeak\_presented)} \quad (4)$$

where *peak intercepted flowrate* is the maximum flowrates observed during that event, and *peak presented flowrate* is the maximum expected flowrates derived from the SWMM model using tributary drainage area characteristics as per design drawings.

3. Results

This section first presents the precipitation and water level data collected at both sites. Then, flowrates to the inlet calculated using the SWMM model and intercepted flowrates for all four inlets are presented. Third, the inlet efficiency for these events for each inlet is presented. Finally, *Mean E* and *Peak E* for these four inlets are compared.

3.1. Precipitation—Event Separation

Between the two sites, a total of 103 events were recorded. However, only 52 of these events resulted in total rainfall exceeding 4 mm and were adequately monitored at all four inlets. These events are presented in Figure 3 and are described in greater detail in Appendix A. Note that events are included in the table if precipitation exceeded 4 mm for at least one of the two sites. A full description of the characteristics of these events, including event total, 5 min peak intensity, average intensity, and precipitation duration are listed in Table A1 for Happyland and in Table A2 for Nashville in Appendix A. Overall, for all events, the median total precipitation at Happyland was 17.65 mm whereas the median total precipitation at Nashville was 12.7 mm. The median 5 min intensity was 32 mm/h and at Nashville, it was 15.24 mm/h. The average intensity for all rainfall events was 6.77 mm/h and that at Nashville was 3.75 mm/h. In addition, the median duration was 6 h and that at Nashville was 9 h.

Box plots, depicting seasonal distribution of the event characteristics were created using 14 events during spring, 21 events during summer, and 17 events during fall for the Nashville site and 9 events during spring, 26 events during summer, and 17 events during fall for the Happyland site. The distribution of total precipitation is depicted using boxplots in Figure 3 (top-left), the mean intensity in Figure 3 (bottom-left), 3 min intensity in Figure 3 (top-right), and the total event duration in Figure 3 (bottom-right). Summer had shorter and more intense storms than spring and fall at both sites. The total precipitation, peak 5 min intensity, and mean intensity at Happyland were higher than those at the Nashville site.

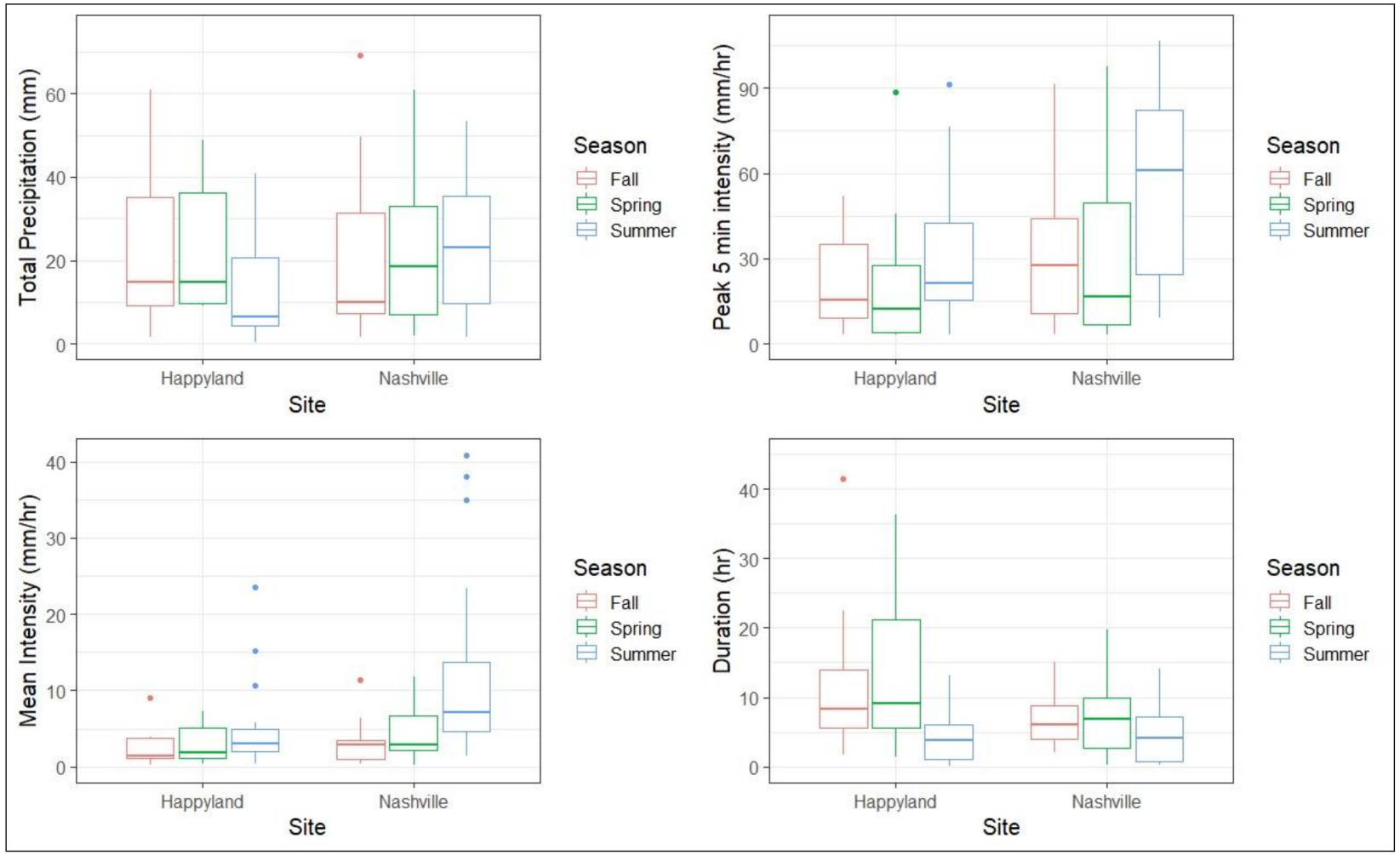

Figure 3. Precipitation characteristics for Happyland and Nashville sites based on common 52 events that occurred during the monitoring period. (Happyland # of events = 14 Spring, 21 Summer, 17 Fall and Nashville # of events = 9 Spring, 26 Summer, 17 Fall).

3.2. The Water Level in the Flume during Precipitation Events

Figure 4 portrays the response of the pressure transducer installed in the Nashville flume to a precipitation event (Event 76). The response of the pressure transducer shows that as the precipitation increases, the water level increases. The peak precipitation intensity matches the peak of the water level, indicating peak flowrate time (all three lines in Figure 4). When the rainfall stops intermittently, the drop in the water level indicates that during that period the flow into the flume reduced. At the beginning of the event, the pressure transducer level (teal and red line) was near zero. At the end of the event, as water stops flowing into the flume approximately after 20 min when the tributary catchment area completely drains into the inlet, the pressure transducer reading of the water level should again be zero. Only applying the calibration equation may not be enough to address this. Thus, in such instances, an additional curation procedure as explained earlier in quality protocol was adopted. A constant (here 0.05 m) was deducted from the calibrated water level.

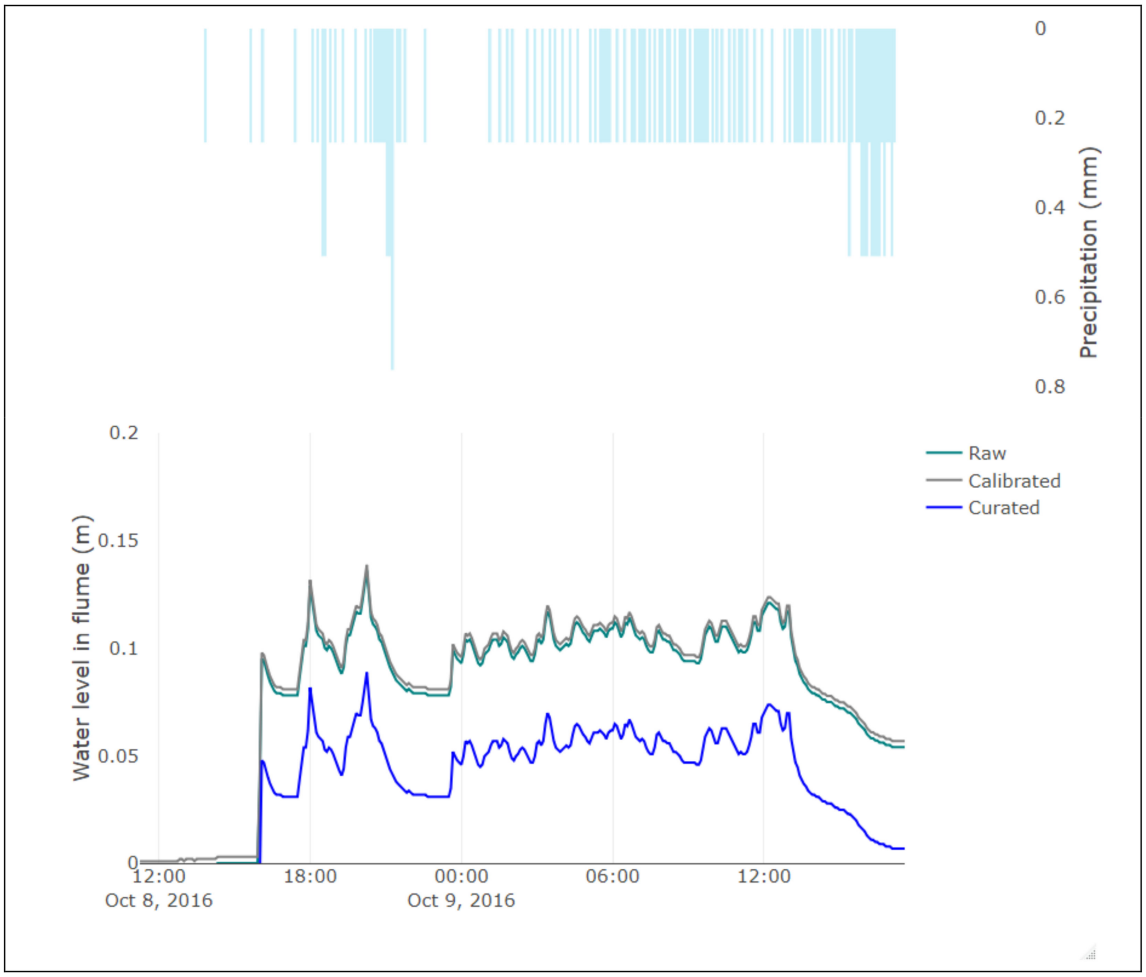

Figure 4. Response of pressure transducer to precipitation event (Event #76) illustrating calibration and data curation.

3.3. Runoff and Intercepted Flowrates

The distribution of runoff and intercepted flowrates that occurred during each event is shown as a boxplot in Figure 5. The intercepted flowrates calculated using the pressure transducer data and flume equation (during events) for the monitoring period are presented in Figure A4a,b included in Appendix A.

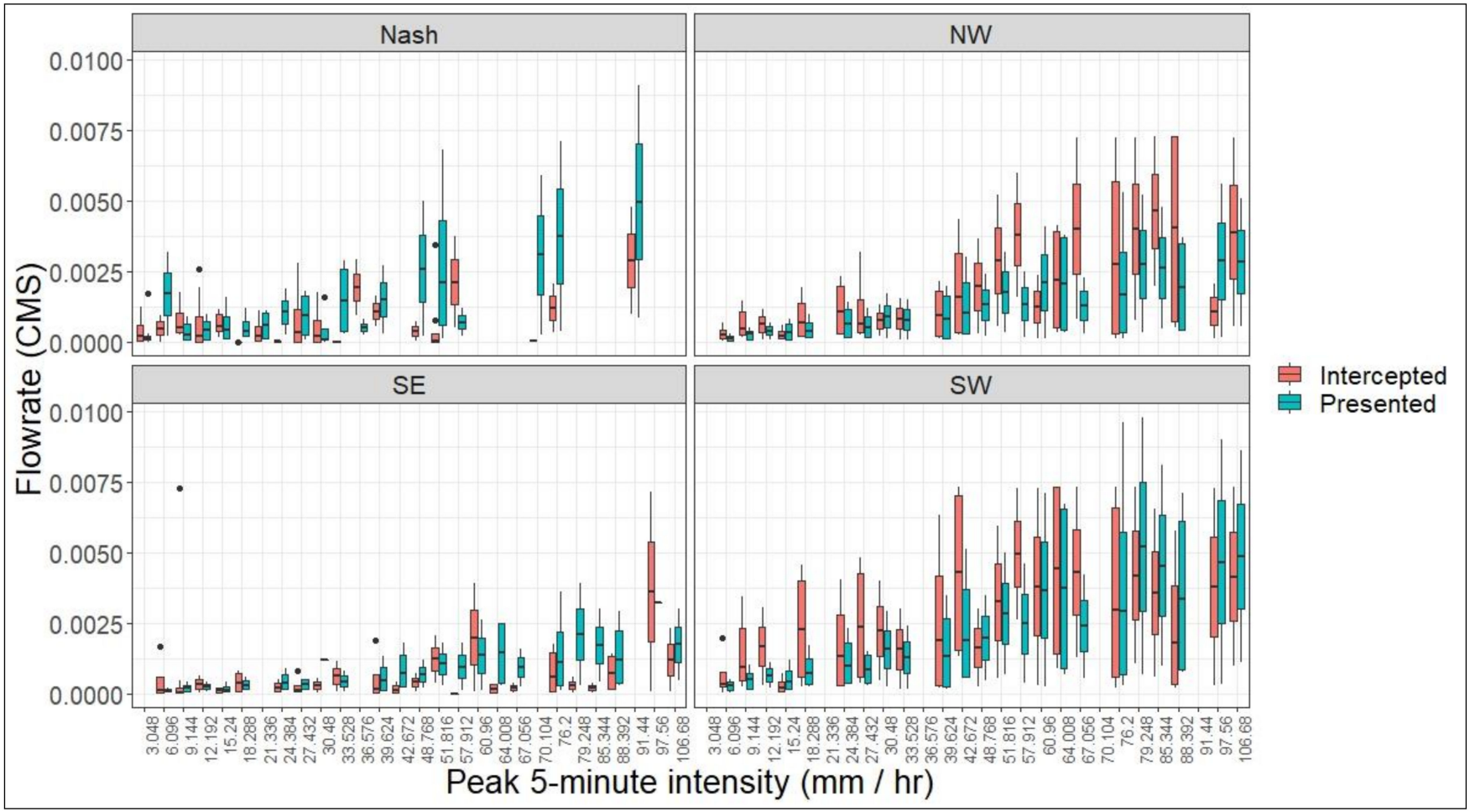

Figure 5. The distribution of presented flowrate and intercepted flowrate for all inlets ranked in order of lowest to highest peak 5 min intensity.

Figure 5 includes side-by-side box plots of the presented flowrates and intercepted flowrates for each storm at each inlet. The boxes represent the distribution of flows that occurred during each respective hydrograph. The pairs of boxes are ranked in order of increasing event precipitation peak 5 min intensity.

The higher peak intensity results in higher presented flowrates. As presented flowrates increase beyond inlet capacity, the intercepted flowrates lower [1,22]. At SW, Nashville, and SE inlets, the intercepted flowrate deceases for the events with higher peak intensity. In contrast to this, at NW site as the intensity increases the intercepted flowrate increases. SW inlet is upstream of NW inlet. As depicted in Figure 5 (bottom-right), the intercepted flowrate is lower than the presented flowrate for events with higher peak intensity. The flowrate that is not intercepted by SW inlet is presented to NW as an additional flowrate inlet as shown in Figure 5 (top-right).

Figure 6a depicts Happyland precipitation Event dated 21 October 2016; total precipitation = 69 mm, maximum intensity = 64 mm/h, average intensity = 10 mm/h. Figure 6b portrays the Nashville precipitation Event dated 21 October 2016; total precipitation = 27 mm, maximum intensity = 27 mm/h, average intensity = 3.6 mm/h. Figure 6c depicts modeled presented flowrate and observed flowrate for Happyland NW and Nashville inlet for these precipitations events described above. Both modeled and observed flowrates follow the precipitation pattern. As the tributary catchment area is impervious, both modeled and observed runoff hydrographs peak within a few minutes after peak intense precipitation. The modeled and observed runoff hydrograph shows two peaks as response to double peaked precipitation for Nashville.

Figure 7 presents investigation of NW, SE, and SW inlets for Event 52—Precipitation recorded at site = 69 mm, average intensity = 10 mm/h, duration = 6 h, peak intensity = 64 mm/h (6 h, 2-year recurrence interval). Figure 7b shows response of NW inlet. The peak intensity of 64 mm/h generated 0.004 CMS flowrate over the design tributary catchment area draining into the NW inlet. According to Shevade et al. (2020), the inlet efficiency of 30% was predicted. The intercepted flowrate at 30% efficiency with 10% clogging is 0.0012 CMS, which is marked as the red dotted line in the plot. The additional bypass from the upstream SW inlet is suspected to possibly enter the inlet. Figure 7c shows observed intercepted flow by the SE inlet during Event 52 and expected runoff presented to the inlet. The pressure transducer did not respond during the event. Figure 7d presents the observed intercepted flow by the SW inlet during Event 52 and expected runoff presented to the inlet. SWMM peak flowrate was 0.007 CMS as shown. For that presented flowrate, 60% inlet efficiency with 10% clogging was predicted by Shevade et al. (2020). The predicted intercepted flowrate = 0.0043 CMS is marked as the red dotted line in the plot.

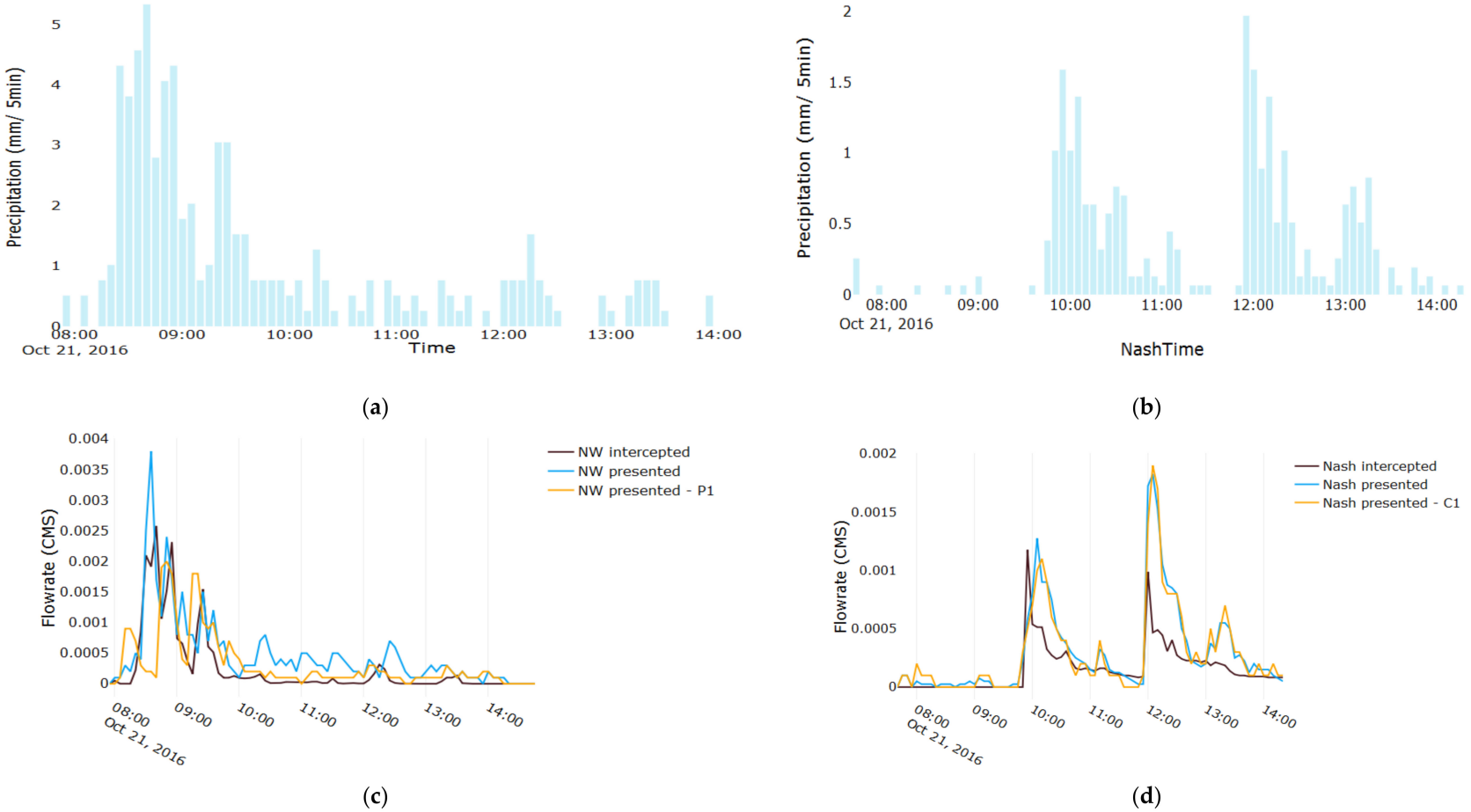

Figure 6. (**a**) On-site precipitation data for Happyland site and (**b**) on-site precipitation data for Nashville site. (**c**,**d**) presented and intercepted flowrates for NW and Nashville inlets. The runoff flowrates presented to the inlets were calculated using SWMM model. The runoff was calculated using reference precipitation gauges (P1 and C1 marked as orange lines) and on-site rain gauge data (marked as blue line). The black line is observed inflow at site.

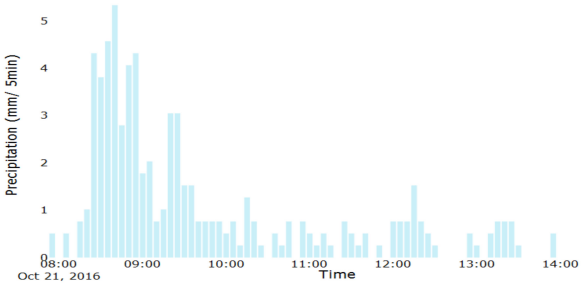

(**a**)

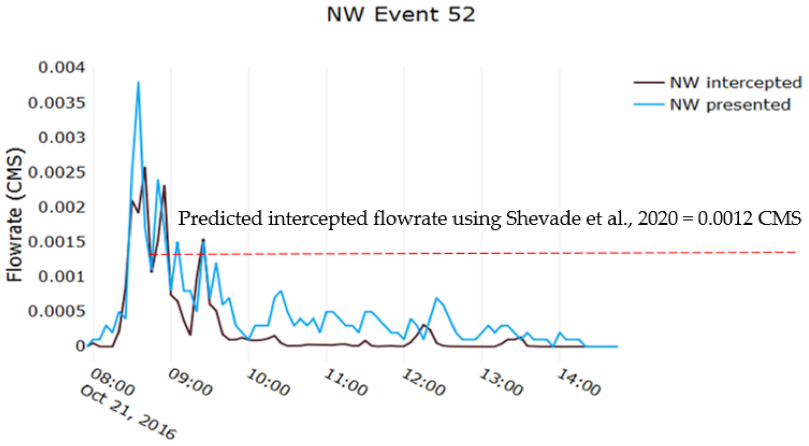

(**b**)

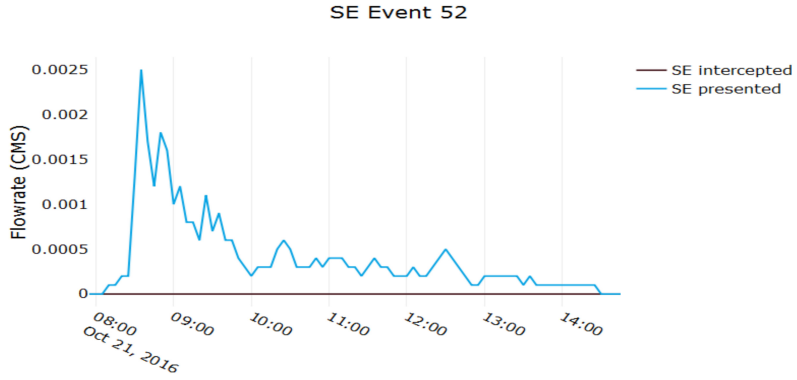

(**c**)

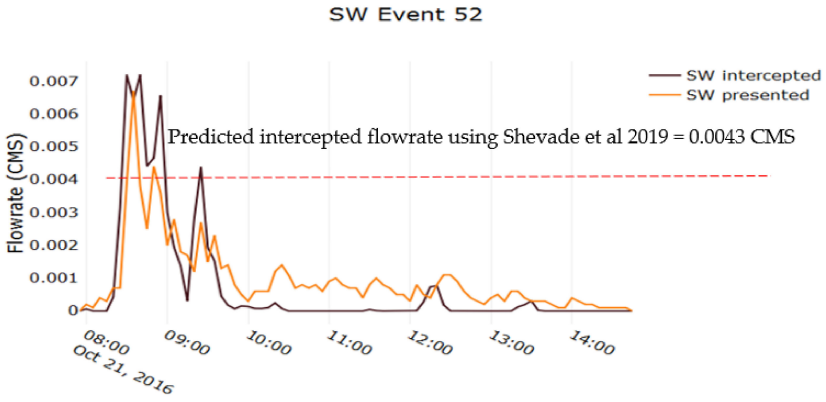

(**d**)

Figure 7. (**a**) Precipitation recorded at site and (**b**–**d**) comparisons of observed inflow (intercepted by inlet) flowrate and estimated presented inflow flowrate over the tributary catchment areas for respective inlets at the Happyland site (inlets NW, SE, and SW) during Event 52.

4. Discussion

The data presented above were quantitatively and qualitatively investigated to explain the inlet behavior. Additionally, individual event flowrate data were evaluated based on the inlet capacities of NW and SW inlets that were calculated using the model described in Shevade et al., 2020 [16].

Though all four inlets had the same physical inlet length, channel length, flume, measuring devices such as flume and pressure transducers, and depth, the apron slope, precipitation characteristics, and tributary catchment area characteristics were different. The effects of these parameters on the efficiency of these four inlets are compared below.

At the SW and NW inlets, the intercepted flowrates generally exceeded the presented flowrates, with a moderate trend of increasing flowrates with greater precipitation visually evident in the figure. The fact that the intercepted flowrates were typically skewed higher than the presented flowrates may suggest that the tributary areas of the NW and SW inlets were greater than those estimated on the design drawings.

By contrast, for most of the events, the intercepted flowrates at the SE inlet were lower than the presented flowrate calculated using the design tributary drainage area during most of the events. Though the inlet had an apron, the street sloped away from the inlet, suggesting that much of the presented flowrate was actually diverted away from the inlet (see Figure 8).

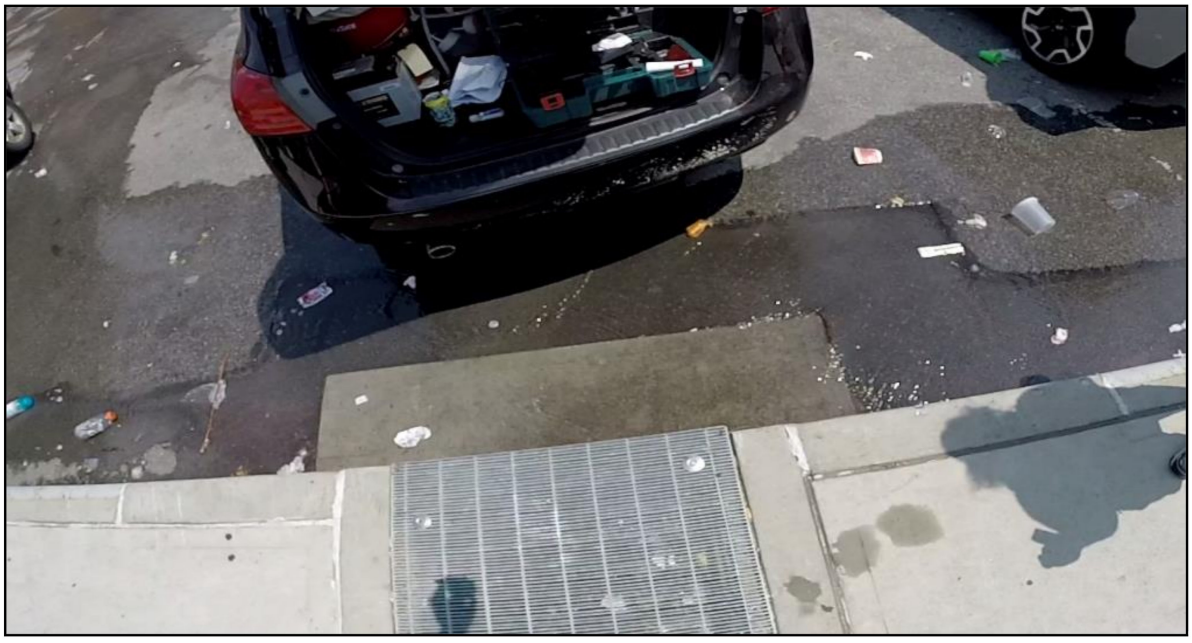

Figure 8. Photograph of SE inlet showing bypass at site.

4.1. Effect of Apron Slope on Inlet Efficiency

Figure 9 compares the mean inlet efficiency calculated using distribution of presented and intercepted flowrates for all events at each inlet using boxplots. The vertical axis is a log scale and the data are organized from highest to lowest apron slope. The two inlets with the steepest apron slopes (NW @ 10% and SW @ 15%) showed the highest mean inlet efficiency. The two inlets with milder apron slopes (SE @ 7% and Nash @ 0%) posted lower efficiencies. Apron slope is known to be a determinant of inlet efficiency [21,22].

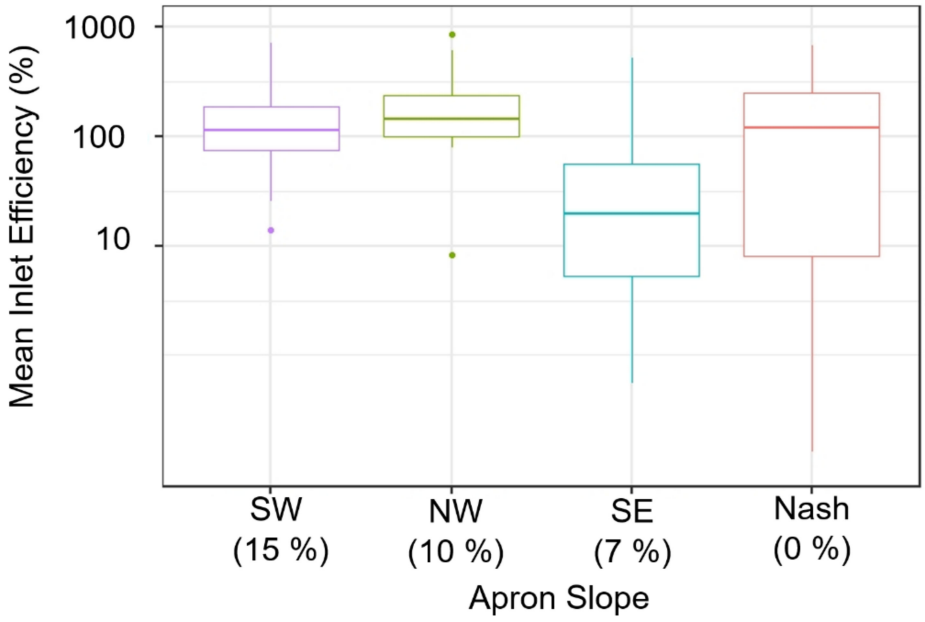

(**a**)

(**b**)

(**c**)

Figure 9. (**a**) Effect of apron slope on mean inlet efficiency of inlets; (**b**) photograph depicting apron conditions at Nashville inlet—0% design apron slope; (**c**) photograph depicting apron conditions at SW inlet—10% design apron slope.

According to the design drawings, the designed apron slope for SW, NW, and SE inlets is 10%. However, field surveying suggests that post-construction street resurfacing and sediment build up reduced the effective slopes of NW and SE aprons. Despite this observation, the NW inlet still yielded the highest mean inlet efficiency. One potential explanation is that even though its apron slope had been compromised, the NW inlet was routinely presented with its own tributary runoff and bypass from the SW inlet, which was located 50 m further upstream. The SW inlet bypass was not considered in the SWMM modeling of the presented flowrate to the NW inlet, which could have resulted in a mean E that was artificially inflated for the NW inlet.

4.2. Effect of Tributary Drainage Area on Peak Inlet Efficiency

Figure 10 compares the peak inlet efficiency calculated using distribution of presented and intercepted flowrates for all events at each inlet using box plots. The vertical axis is a log scale and data are organized ranked from highest to lowest tributary drainage area. The inlet with the largest tributary drainage area (SW—650 m^2) showed the highest mean inlet efficiency (SW—650 m^2). The tributary drainage area for NW inlet was 325 m^2 (much lower than SW inlet); the peak inlet efficiency was still higher. This is due to the possibility of bypass from the upstream SW inlet entering into the inlet. This is not captured in the

SWMM model, thus inflating the peak inlet efficiency artificially. The tributary drainage area for SE inlet was 278 m^2 (lowest in this study). The tributary drainage area for Nashville inlet was 475 m^2 (second largest in this study). SE and Nashville inlets had peak inlet efficiency less than 100% for 50% of the events. The other drainage area characteristics such as the quasi-orthogonal flow at this inlet and a higher street slope, 4.75% (>2.5%) were different than at the other three inlets.

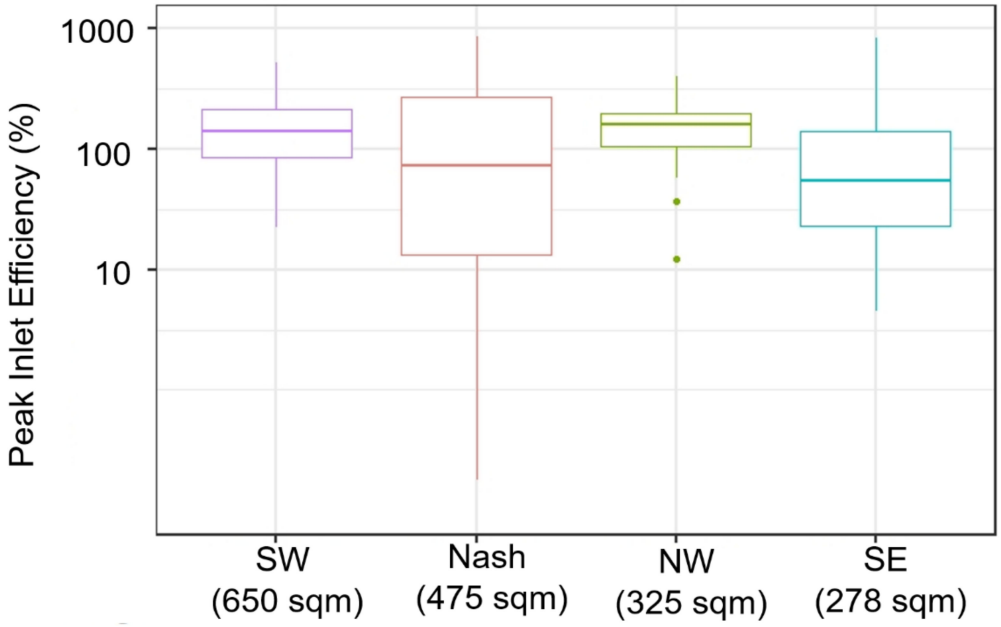

Figure 10. Effect of tributary drainage area on peak inlet efficiency.

4.3. Effect of Season on Mean and Peak Inlet Efficiency

The mean inlet efficiency (calculated for all events) for all sites is presented in Figure 11a. The mean inlet efficiency computed in the fall season is lower than in the spring and summer for Nashville, SE, and NW sites, perhaps due to the clogging of the inlets with leaves in the autumn (see Figure 11b).

Nashville had greater variability of mean inlet efficiency during fall. The SW inlet still showed better efficiency than the other inlets, perhaps because of its higher apron slope and also the possibility that its drainage area, too, was underestimated in the SWMM model, as catchbasins located further upstream bypassed presenting the inlet with more flow.

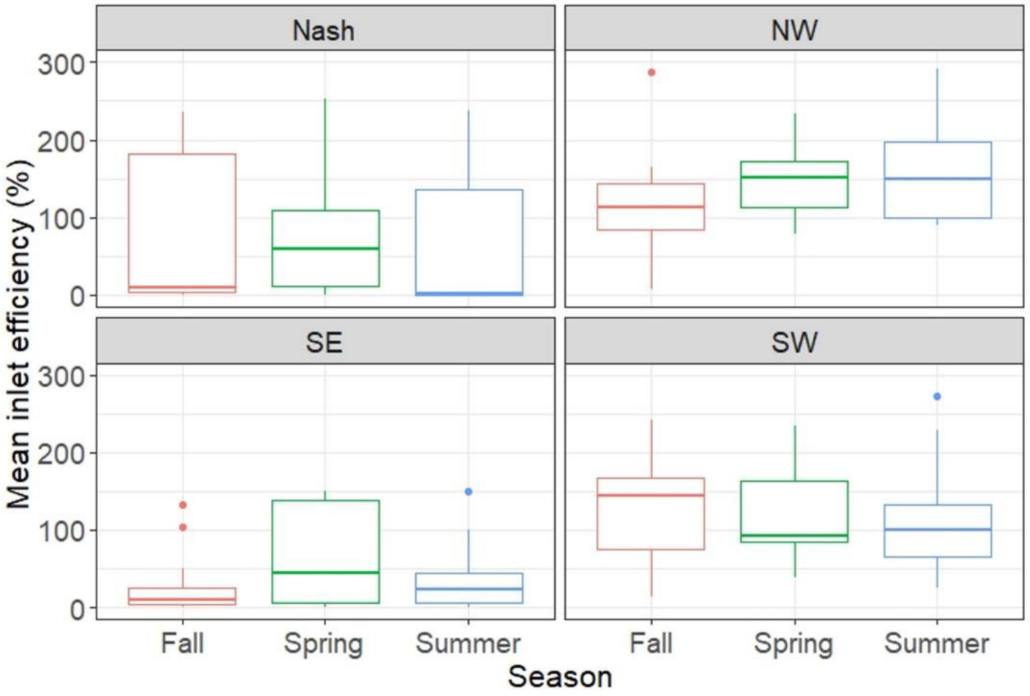

(**a**)

(**b**)

Figure 11. (**a**) Effect of season on mean inlet efficiency; (**b**) leaves collected during fall reducing mean inlet efficiency during season.

5. Conclusions

The microclimate varies within the city, and precipitation characteristics such as intensity, duration, start time, and total depth vary from one site to another. One part of

the city may receive higher intense rain than another. Thus, more GI should be placed in such parts of cities. In NYC, Bronx receives higher precipitation, both total rainfall and intensity, than Queens. The construction of GI in Bronx should be prioritized.

Small-scale spatial variability of rainfall, measurement uncertainty, tributary drainage area characteristics and uncertainty, and local inlet depression were all identified as potential determinants of observed inlet efficiency. With these caveats, the research presented here suggests a moderate visual correlation between increasing apron slope and better inlet efficiency. The effect of local depression (apron slope) on inlet efficiency, higher presented flowrate, and clogging were studied in the previous work published in Shevade et al., 2020. The effect of each of these factors was isolated by keeping other factors constant during simulations. Such additional work is needed to disentangle confounding factors associated with measurement uncertainty, differences between the designed and as-built, present-day conditions of the site, and the frequency with which sediment blocks the inlet.

The actual tributary drainage area presenting flow to the inlet can vary from event to event for the same inlet due to such differences. If upstream inlets are clogged, bypass from those inlets can contribute as additional flow to downstream inlets. These bypass flowrates would not be represented in runoff simulations as such were performed here using SWMM. These kinds of factors are likely responsible for inaccuracies in the inlet efficiencies that were computed here.

GI site with one inlet was less effective in capturing higher flowrates than GI site with multiple inlets. Though the inlet capacity of NW inlet (0.00044 CMS) was less than that of SW inlet (0.00052 CMS), NW inlet intercepted equal or more flowrate during most of the events than SW inlet. As it was placed downstream of SW inlet, it was always presented with more than design flowrate. For better utilization of GI storage, the inlet design and placement of inlets should be selected carefully.

The seasonal variability of inlet performance arises due to the climatological and seasonal maintenance requirements. The observed seasonal variability in inlet performance requires additional study.

Author Contributions: Conceptualization, methodology, visualization, software, validation, formal analysis, investigation, resources, data curation, and writing—original draft preparation, L.J.S.; writing—review and editing, supervision, funding acquisition, F.A.M. All authors have read and agreed to the published version of the manuscript.

Funding: Significant funding for the stormwater capture green street project site referenced in this article was provided by the NYS Attorney General under the Bronx River Watershed Initiative through a grant #34724 "The Happyland Memorial Garden Expansion". This research was also partially funded by the National Science Foundation through CAREER: Integrated Assessments of the Impacts of Decentralized Land Use and Water Management (CBET: 1150994), and the National Oceanic and Atmospheric Association (NOAA) through Supporting Regional Implementation of Integrated Climate Resilience: Consortium for Climate Risks in the Urban Northeast (CCRUN) Phase II (NA15OAR4310147), the National Science Foundation's Coastal SEES program (CMMI 1325676). The cost of publication was shared by Lafayette College and Drexel University.

Institutional Review Board Statement: Not applicable.

Informed Consent Statement: Not applicable.

Data Availability Statement: The data presented in this study are available on request from the corresponding author.

Acknowledgments: The authors would like to thank NYC Department of Parks and Recreation and NYC—Department of Environmental Protection. The authors would also like to thank Qi Long Chen from NYC—DEP, Julian Stolper, Nathan Caplan, Noah Katz, Brandon James, SWRE Laboratory field technicians, and other lab members for helping to conduct the field experiments and maintaining site monitoring equipment.

Conflicts of Interest: The authors declare no conflict of interest.

Appendix A

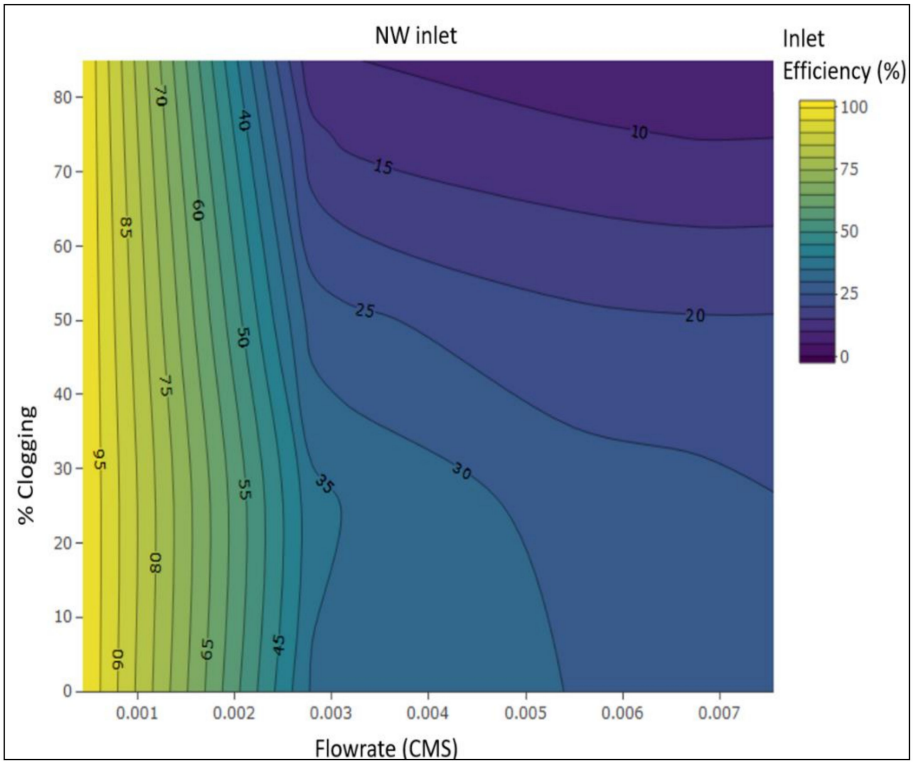

Figure A1. (Reprinted from Shevade et al., 2020). Effect of increased flowrate and inlet clogging on inlet efficiency for NW inlet.

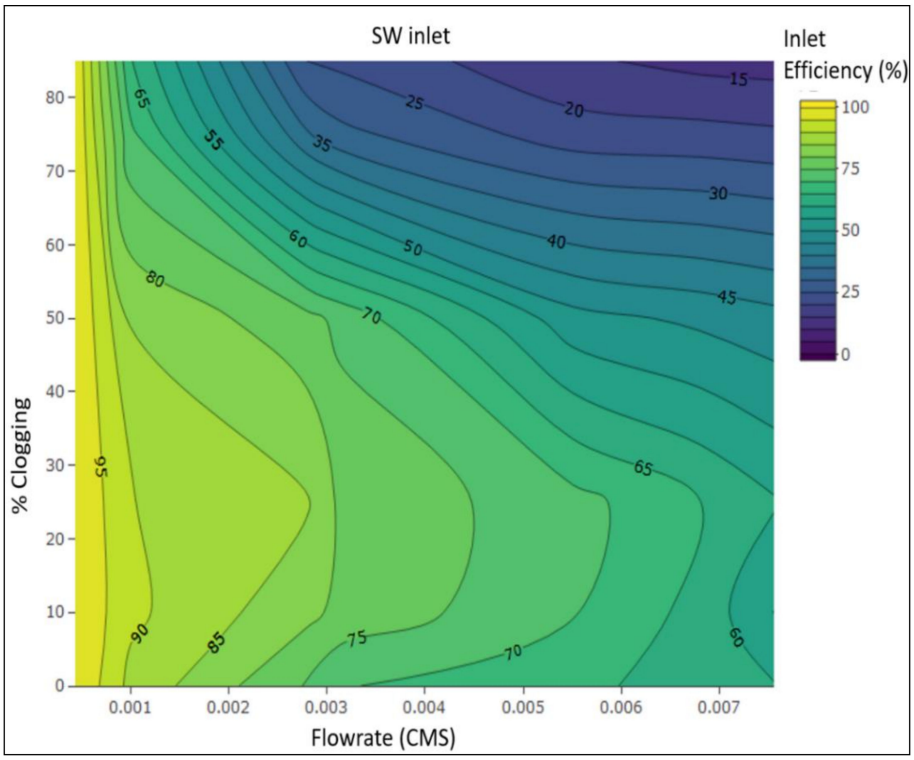

Figure A2. (Reprinted from Shevade et al., 2020). Effect of increased flowrate and inlet clogging on inlet efficiency for SW inlet.

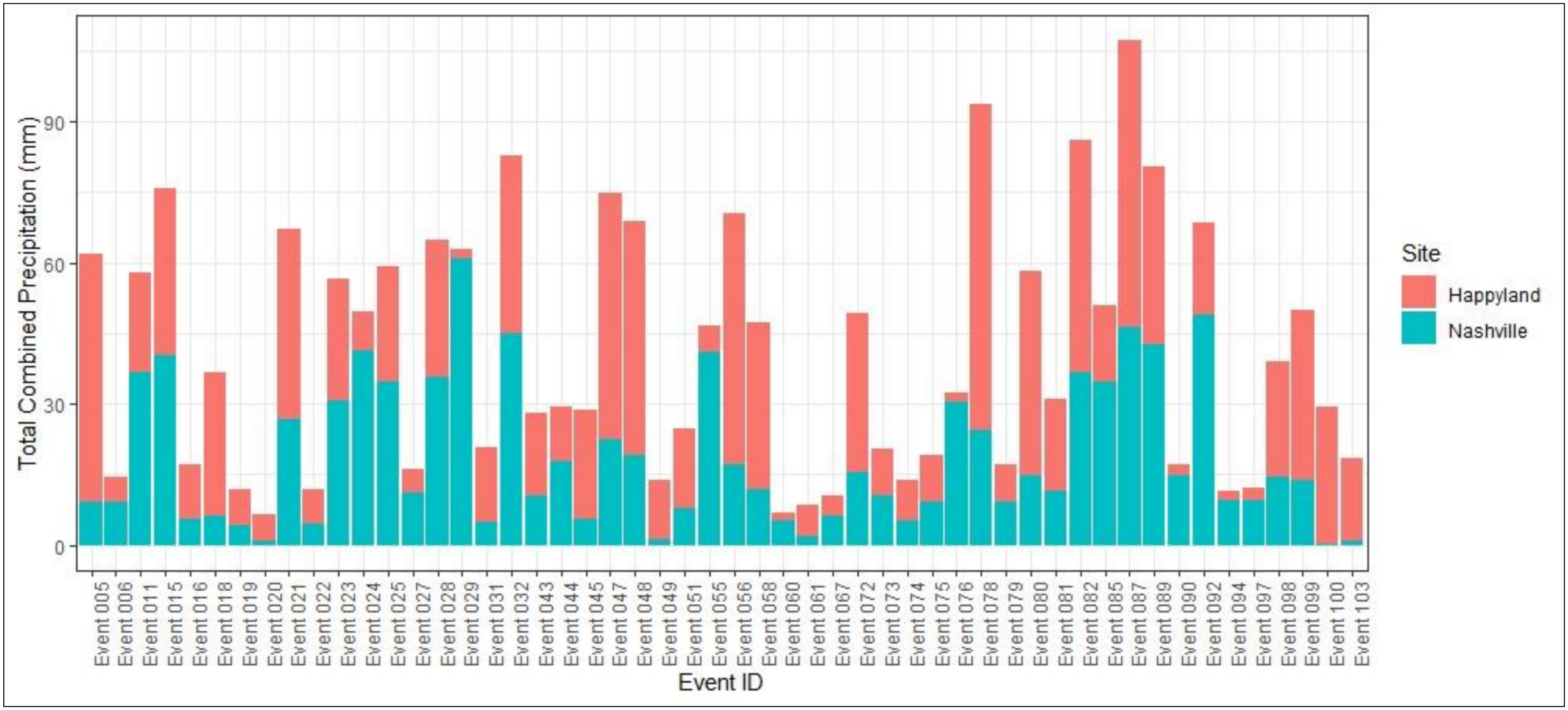

Figure A3. Total precipitation at Happyland and Nashville sites based on common 52 events that occurred during the monitoring period.

Table A1. Precipitation events at Happyland site.

Event ID	Start	End	Total Rain (mm)	PeakH5 (mm/h)	Duration (h)	Mean Intensity (mm/h)
Event 005	5/31/2015 15:35	6/1/2015 10:30	52.58	42.67	19.00	2.77
Event 006	6/1/2015 18:40	6/2/2015 8:40	5.33	6.10	14.08	0.38
Event 011	6/14/2015 21:30	6/15/2015 4:25	21.08	51.82	7.00	3.01
Event 015	6/27/2015 15:15	6/28/2015 5:20	35.31	9.14	14.17	2.49
Event 016	7/1/2015 3:40	7/1/2015 3:55	11.68	85.34	0.33	35.05
Event 018	7/14/2015 12:10	7/14/2015 13:55	30.23	88.39	1.83	16.49
Event 019	7/18/2015 7:05	7/18/2015 8:00	7.62	24.38	1.00	7.62
Event 020	7/27/2015 2:15	7/27/2015 2:50	5.59	24.38	0.67	8.38
Event 021	7/30/2015 8:10	7/30/2015 16:20	40.39	85.34	8.25	4.90
Event 022	8/4/2015 2:50	8/4/2015 3:30	7.37	48.77	0.75	9.82
Event 023	8/11/2015 3:30	8/11/2015 10:25	25.91	24.38	7.00	3.70
Event 024	8/21/2015 0:40	8/21/2015 3:10	8.38	15.24	2.58	3.24
Event 025	9/10/2015 0:30	9/10/2015 9:00	24.64	33.53	8.58	2.87
Event 027	9/12/2015 18:20	9/12/2015 23:15	5.08	15.24	5.00	1.02
Event 028	9/29/2015 21:40	9/30/2015 6:40	28.96	73.15	9.08	3.19
Event 029	10/1/2015 17:20	10/1/2015 20:20	1.78	3.05	3.08	0.58
Event 031	10/9/2015 11:50	10/9/2015 17:50	16.00	45.72	6.08	2.63
Event 032	10/28/2015 10:15	10/29/2015 1:15	37.85	39.62	15.08	2.51
Event 043	6/5/2016 17:40	6/5/2016 19:05	17.78	76.20	1.50	11.85
Event 044	6/8/2016 12:00	6/8/2016 14:55	11.68	9.14	3.00	3.89
Event 045	6/27/2016 20:40	6/28/2016 0:40	23.11	42.67	4.08	5.66
Event 047	7/1/2016 16:40	7/1/2016 21:25	52.33	97.56	4.83	10.83
Event 048	7/4/2016 20:05	7/5/2016 5:00	49.78	64.01	9.00	5.53
Event 049	7/7/2016 13:30	7/7/2016 13:45	12.70	76.20	0.33	38.10
Event 051	7/14/2016 15:15	7/14/2016 15:35	17.02	106.68	0.42	40.84
Event 055	7/25/2016 14:55	7/25/2016 18:55	5.84	15.24	4.08	1.43
Event 056	7/29/2016 0:15	7/29/2016 7:40	53.34	67.06	7.50	7.11
Event 058	7/31/2016 17:00	7/31/2016 23:55	35.56	79.25	7.00	5.08
Event 060	8/10/2016 12:15	8/10/2016 12:35	1.78	9.14	0.42	4.27
Event 061	8/11/2016 23:10	8/12/2016 1:05	6.60	9.14	2.00	3.30
Event 067	9/1/2016 4:25	9/1/2016 13:05	4.06	6.10	8.75	0.46
Event 072	9/19/2016 4:25	9/19/2016 11:00	33.78	91.44	6.67	5.07
Event 073	9/23/2016 23:30	9/24/2016 5:00	9.91	18.29	5.58	1.77
Event 074	9/27/2016 1:40	9/27/2016 4:20	8.89	27.43	2.75	3.23
Event 075	9/30/2016 11:45	9/30/2016 23:30	9.91	9.14	11.83	0.84
Event 076	10/8/2016 13:45	10/8/2016 18:55	2.29	6.10	5.25	0.44
Event 078	10/21/2016 7:55	10/21/2016 13:55	69.34	64.01	6.08	11.40
Event 079	10/22/2016 3:25	10/22/2016 12:05	8.13	12.19	8.75	0.93
Event 080	10/27/2016 9:20	10/27/2016 21:25	43.43	30.48	12.17	3.57
Event 081	10/30/2016 15:35	10/30/2016 18:35	19.56	76.20	3.08	6.34
Event 082	11/15/2016 4:00	11/15/2016 12:25	49.53	42.67	8.50	5.83
Event 085	4/25/2017 16:20	4/25/2017 22:35	16.00	18.29	6.33	2.53
Event 087	5/5/2017 6:00	5/5/2017 14:00	60.96	57.91	8.08	7.54
Event 089	5/13/2017 4:00	5/13/2017 23:35	37.85	6.10	19.67	1.92
Event 090	5/22/2017 2:50	5/22/2017 3:40	2.03	6.10	0.92	2.22
Event 092	5/25/2017 4:25	5/25/2017 13:45	19.56	9.14	9.42	2.08
Event 094	5/29/2017 3:30	5/29/2017 10:10	2.03	3.05	6.75	0.30
Event 097	6/14/2017 3:40	6/14/2017 3:55	2.79	15.24	0.33	8.38
Event 098	6/17/2017 11:15	6/17/2017 13:50	24.38	30.48	2.67	9.14
Event 099	6/19/2017 16:55	6/20/2017 2:55	36.07	97.56	10.08	3.58
Event 100	6/23/2017 22:30	6/24/2017 8:40	29.21	39.62	10.25	2.85
Event 103	7/3/2017 22:55	7/3/2017 23:35	17.53	60.96	0.75	23.37

Table A2. Precipitation events at Nashville site.

Event ID	Start	End	Total Rain (mm)	PeakH5 (mm/h)	Duration (h)	Mean Intensity (mm/h)
Event 005	5/31/2015 17:00	5/31/2015 22:05	9.14	27.43	5.17	1.77
Event 006	6/1/2015 9:40	6/1/2015 11:30	9.14	12.19	1.92	4.77
Event 011	6/14/2015 21:20	6/15/2015 4:05	36.83	45.72	6.83	5.39
Event 015	6/27/2015 15:05	6/28/2015 4:10	40.39	24.38	13.17	3.07
Event 016	7/1/2015 3:35	7/1/2015 4:40	5.59	18.29	1.17	4.79
Event 018	7/14/2015 10:25	7/14/2015 16:05	6.35	21.34	5.75	1.10
Event 019	7/18/2015 8:25	7/18/2015 9:10	4.32	33.53	0.83	5.18
Event 020	7/27/2015 2:25	7/27/2015 2:35	1.02	6.10	0.25	4.06
Event 021	7/30/2015 8:05	7/30/2015 16:40	26.67	70.10	8.67	3.08
Event 022	8/4/2015 3:20	8/4/2015 5:35	4.57	18.29	2.33	1.96
Event 023	8/11/2015 3:10	8/11/2015 9:30	30.73	33.53	6.42	4.79
Event 024	8/21/2015 0:40	8/21/2015 5:10	41.15	51.82	4.58	8.98
Event 025	9/9/2015 23:15	9/10/2015 17:40	34.54	51.82	18.50	1.87
Event 027	9/12/2015 16:20	9/13/2015 0:35	11.18	30.48	8.33	1.34
Event 028	9/29/2015 22:05	9/30/2015 13:15	35.81	48.77	15.25	2.35
Event 029	10/1/2015 15:00	10/3/2015 8:25	60.96	12.19	41.50	1.47
Event 031	10/10/2015 0:45	10/10/2015 5:15	4.83	51.82	4.58	1.05
Event 032	10/28/2015 23:40	10/29/2015 11:25	44.96	6.10	11.83	3.80
Event 043	6/5/2016 18:00	6/5/2016 19:20	10.41	36.58	1.42	7.35
Event 044	6/8/2016 11:45	6/8/2016 15:05	17.78	15.24	3.42	5.20
Event 045	6/27/2016 21:15	6/28/2016 1:40	5.59	3.05	4.50	1.24
Event 047	7/1/2016 16:50	7/1/2016 21:45	22.35	57.91	5.00	4.47
Event 048	7/4/2016 22:30	7/5/2016 5:35	19.05	15.24	7.17	2.66
Event 049	7/7/2016 14:35	7/7/2016 14:35	1.27	15.24	0.08	15.24
Event 051	7/14/2016 15:40	7/14/2016 15:55	7.87	51.82	0.33	23.62
Event 055	7/25/2016 15:45	7/25/2016 19:30	40.89	91.44	3.83	10.67
Event 056	7/29/2016 0:10	7/29/2016 8:45	17.02	21.34	8.67	1.96
Event 058	7/31/2016 21:25	7/31/2016 23:20	11.68	76.20	2.00	5.84
Event 060	8/10/2016 12:20	8/10/2016 17:35	5.08	15.24	5.33	0.95
Event 061	8/11/2016 17:30	8/12/2016 0:55	1.78	3.05	7.50	0.24
Event 067	9/1/2016 14:00	9/1/2016 15:35	6.35	12.19	1.67	3.81
Event 072	9/19/2016 4:50	9/19/2016 12:00	15.49	9.14	7.25	2.14
Event 073	9/24/2016 0:10	9/24/2016 8:00	10.41	15.24	7.92	1.32
Event 074	9/27/2016 1:35	9/27/2016 6:15	5.08	15.24	4.75	1.07
Event 075	9/30/2016 9:05	9/30/2016 22:00	9.14	12.19	13.00	0.70
Event 076	10/8/2016 15:15	10/9/2016 13:35	30.23	9.14	22.42	1.35
Event 078	10/21/2016 7:40	10/21/2016 13:55	24.38	27.43	6.33	3.85
Event 079	10/22/2016 4:15	10/22/2016 13:15	9.14	9.14	9.08	1.01
Event 080	10/27/2016 9:35	10/28/2016 0:20	14.73	9.14	14.83	0.99
Event 081	10/30/2016 15:55	10/30/2016 18:45	11.43	39.62	2.92	3.92
Event 082	11/15/2016 2:25	11/15/2016 11:55	36.58	30.48	9.58	3.82
Event 085	4/25/2017 2:35	4/26/2017 10:00	34.80	27.43	31.50	1.10
Event 087	5/5/2017 6:35	5/5/2017 13:50	46.23	88.39	7.33	6.30
Event 089	5/13/2017 3:40	5/14/2017 0:25	42.67	9.14	20.83	2.05
Event 090	5/22/2017 8:00	5/22/2017 17:50	14.99	6.10	9.92	1.51
Event 092	5/25/2017 4:00	5/26/2017 6:00	48.77	12.19	26.08	1.87
Event 094	5/29/2017 3:20	5/29/2017 12:10	9.40	3.05	8.92	1.05
Event 097	6/14/2017 5:30	6/14/2017 14:40	9.40	3.05	9.25	1.02
Event 098	6/17/2017 11:45	6/18/2017 8:55	14.48	3.05	21.25	0.68
Event 099	6/19/2017 18:10	6/21/2017 6:25	13.72	3.05	36.33	0.38
Event 100	6/24/2017 2:25	6/24/2017 2:25	0.25	3.05	0.08	3.05
Event 103	7/3/2017 16:20	7/3/2017 18:55	1.02	3.05	2.67	0.38

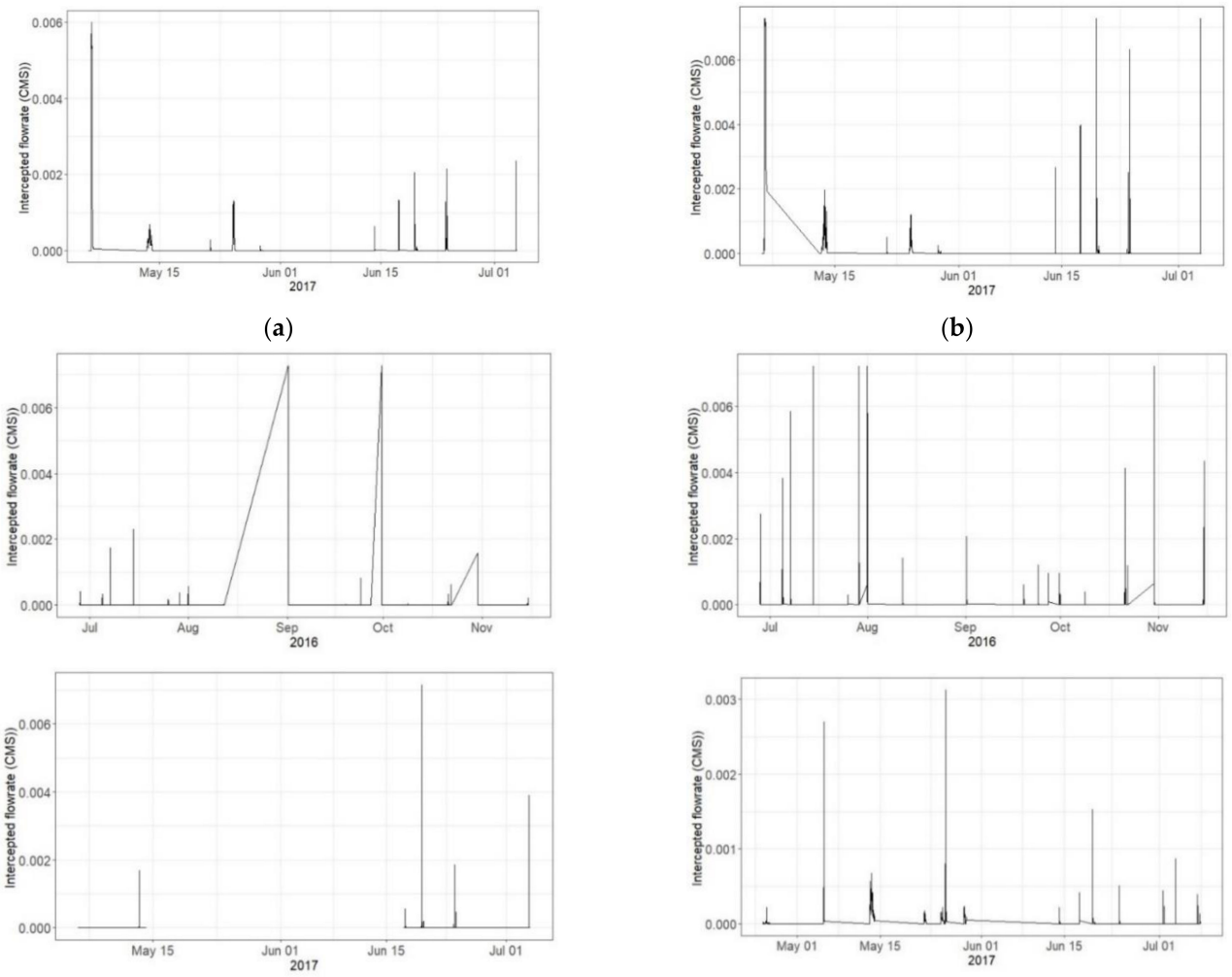

Figure A4. Intercepted flowrate for all inlets during monitoring period. (**a**) NW inlet (**b**) SW inlet (**c**) SE inlet (**d**) Nashville inlet.

References

1. Jia, H.; Yao, H.; Tang, Y.; Yu, S.L.; Field, R.; Tafuri, A.N. LID-BMPs planning for urban runoff control and the case study in China. *J. Environ. Manag.* **2015**, *149*, 65–76. [CrossRef]
2. NAE. Grand Challenges for Engineering in the 21st Century. 2008. Available online: http://www.engineeringchallenges.org/challenges/infrastructure.aspx (accessed on 15 January 2019).
3. Cording, A.; Hurley, S.; Whitney, D. Monitoring methods and designs for evaluating bioretention performance. *J. Environ. Eng.* **2017**, *143*, 05017006. [CrossRef]
4. Lewellyn, C.; Lyons, C.E.; Traver, R.G.; Wadzuk, B.M. Evaluation of seasonal and large storm runoff volume capture of an infiltration green infrastructure system. *J. Hydrol. Eng.* **2016**, *21*, 04015047. [CrossRef]
5. Jaber, F.H. Bioretention and permeable pavement performance in clay soil. In Proceedings of the International Low Impact Development Conference 2015—LID, IT Works in all Climates and Soils, Houston, TX, USA, 19–21 January 2015; American Society of Civil Engineers: Reston, VA, USA, 2015; pp. 151–160.
6. Asleson, B.C.; Nestingen, R.S.; Gulliver, J.; Hozalski, R.; Nieber, J.L. Performance Assessment of Rain Gardens. *J. Am. Water Resour. Assoc.* **2009**, *45*, 1019–1031. [CrossRef]
7. Brown, R.A.; Hunt, W.F. Impacts of media depth on effluent water quality and hydrologic performance of under-sized bioretention cells. *J. Water Environ. Res.* **2011**, *137*, 132–143.
8. Davis, A.P.; Traver, R.G.; Hunt, W.F.; Lee, R.; Brown, R.A.; Olszewski, J.M. Hydrologic performance of bioretention storm-water control measures. *J. Hydrol. Eng.* **2012**, *17*, 604–614. [CrossRef]
9. Hsieh, C.-H.; Davis, A.P. Multiple-event study of bioretention for treatment of urban storm water runoff. *Water Sci. Technol.* **2005**, *51*, 177–181. [CrossRef]

10. Ahmed, F.; Gulliver, J.; Nieber, J. Field infiltration measurements in grassed roadside drainage ditches: Spatial and temporal variability. *J. Hydrol.* **2015**, *530*, 604–611. [CrossRef]
11. Braga, A.; Horst, M.; Traver, R.G. Temperature effects on the infiltration rate through an infiltration basin BMP. *J. Water Environ. Res.* **2007**, *133*, 593–601. [CrossRef]
12. Alizadehtazi, B.; DiGiovanni, K.; Foti, R.; Morin, T.; Shetty, N.H.; Montalto, F.A.; Gurian, P.L. Comparison of observed infiltration rates of different permeable urban surfaces using a cornell sprinkle infiltrometer. *J. Hydrol. Eng.* **2016**, *21*, 06016003. [CrossRef]
13. DiGiovanni, K.A. Evapotranspiration from Urban Green Spaces in Northeast United States City. Ph.D. Thesis, Drexel University, Philadelphia, PA, USA, 2013.
14. Small-Mantey, L.A. The Potential Role of Green Infrastructure in Mitigation of the Urban Heat Island Effect. Ph.D. Thesis, Drexel University, Philadelphia, PA, USA, 2017.
15. De'Sousa, M.R.S.; Montalto, F.A.; Gurian, P. Evaluating green infrastructure stormwater capture perfor-mance under extreme precipitation. *J. Extrem. Events* **2016**, *3*, 1650006. [CrossRef]
16. Shevade, L.J.; Lo, L.J.; Montalto, F.A. Numerical 3D Model Development and Validation of Curb-Cut Inlet for Efficiency Prediction. *Water* **2020**, *12*, 1791. [CrossRef]
17. Cecinati, F.; De Niet, A.C.; Sawicka, K.; Rico-Ramirez, M.A. Optimal temporal resolution of rainfall for urban applications and uncertainty propagation. *Water* **2017**, *9*, 762. [CrossRef]
18. Habib, E.; Krajewski, W.F.; Kruger, A. Sampling errors of tipping-bucket rain gauge measurements. *J. Hydrol. Eng.* **2001**, *6*, 159–166. [CrossRef]
19. World Meteorological Organization. *Guide to Meteorological Instruments and Methods of Observation*; World Meteorological Organization: Geneva, Switzerland, 2010.
20. Rossman, L.A. *Storm Water Management Model User's Manual*; Version 5.1; US EPA: Washington, DC, USA, 2015.
21. Brown, S.A.; Schall, J.D.; Morris, J.L.; Doherty, C.L.; Stein, S.M.; Warner, J.C. *Urban Drainage Design Manual: Hydraulic Engineering Circular No. 22*, 3rd ed.; Federal Highway Administration: Washington, DC, USA, 2016.
22. Izzard, C.F. Tentative Results on Capacity of Curb Opening Inlets. 1950. Available online: http://onlinepubs.trb.org/Onlinepubs/hrbresearchrpts/1950/11B-004.pdf (accessed on 15 January 2019).